



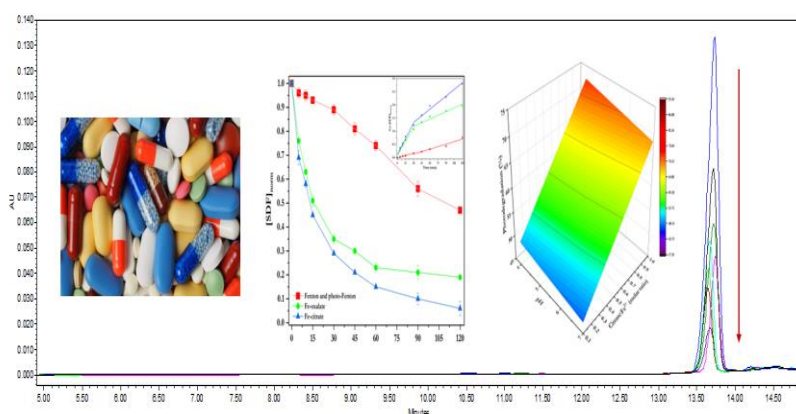
Full Paper | <http://dx.doi.org/10.17807/orbital.v17i1.22735>

Potential of Organic Complexing Agents in Enhancing Fenton and Photo-Fenton Reactions: A Sustainable Approach Using Solar Irradiation for Emerging Contaminants Treatment

Marciele O. Silva^a, Maiara B. Marques ^b, and Danilo R. Souza^a 

This study investigates the influence of organic complexing agents on the Fenton and photo-Fenton reactions to degrade diclofenac sodium (SDF). The effects of adding sodium citrate and sodium oxalate were investigated. A factorial experimental design evaluates pH, irradiation source, and the citrate:Fe²⁺ ratio. Solar photodegradation and acute toxicity tests were conducted to evaluate process performance. HPLC-UV and TOC techniques were monitored diclofenac sodium concentrations, while bioassays with *Artemia salina* assessed toxicity reduction. The results showed that organic complexing agents, particularly sodium citrate, significantly improved photocatalytic efficiency. The experimental design validated the feasibility of using LED lamps for irradiation, demonstrating excellent performance at neutral pH when higher concentrations of sodium citrate were employed. Solar photocatalytic tests showed photodegradation rates exceeding 90%, while TOC and toxicity reduction analyses revealed approximately 80% and 100% efficiencies, respectively. These findings contribute to environmental science by presenting an efficient, sustainable, and adaptable technology for emerging contaminant degradation.

Graphical abstract



Keywords

Emerging contaminants
Fenton and Photo-Fenton
Solar photodegradation
Organic Complexes
Toxicity

Article history

Received 29 Jan 2025
Revised 12 Mar 2025
Accepted 22 Mar 2025
Available online 30 Apr 2025

Handling Editor: Adilson Beatriz

1. Introduction

Emerging contaminants, which include pharmaceuticals, personal care products, industrial chemicals, and agricultural

waste, have gained significant attention in recent decades due to their persistence and potential risks to environmental and

^a Center for Exact Sciences and Technologies - Federal University Western of Bahia; Barreiras, Ba, Brazil. ^b Tocantins State University - Augustinópolis, To, Brazil. *Corresponding author. E-mail: danilo.souza@ufob.edu.br

human health. Previously unmonitored, these compounds are now recognized as a major concern in aquatic and terrestrial ecosystems [1–5].

The key characteristic of emerging contaminants is their environmental persistence and potential adversely affect ecosystems. Many of these compounds resist degradation in groundwater, water bodies, and soils for extended periods [6–15].

The presence of pharmaceutical active compounds (PhACs) in aquatic ecosystems has been known since the mid-20th century. However, recent advancements in analytical technologies and ecological studies have heightened concerns about their impacts. These compounds pose significant risks to aquatic and terrestrial organisms, even at low concentrations, due to their potential for bioaccumulation and long-term exposure. Notable examples include antibiotics, analgesics, β -blockers, hormones, stimulants, antiepileptics, and illicit drugs [4,9,16–19].

Currently, approximately 3,000 compounds are used as pharmaceuticals, with annual production exceeding hundreds of tons. The emergence of new diseases, such as COVID-19, has underscored the importance of research, development, and production of new drugs to maintain and improve public health, making it a global development priority [2,20,21].

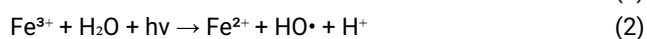
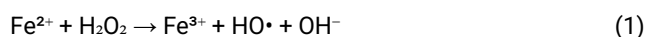
Consequently, the pharmaceutical market remains one of the most significant global industries, generating revenue exceeding 1.12 trillion U.S. dollars in 2022. In Latin America, Brazil stands out as only country among the top global pharmaceutical markets, with a global share of approximately 2.2 % and a market value of nearly 23 billion U.S. dollars [22].

Sodium diclofenac, a widely used nonsteroidal anti-inflammatory drug (NSAID), is effective for pain relief, inflammation reduction, and fever management. It can be administered in various forms, including tablets, ointments, and intravenous injections, making it versatile for treating conditions such as arthritis, muscle pain, migraines, and injuries. In Brazil, its widespread use is driven by its effectiveness, low cost, and high consumption. Studies indicate that approximately 15% of diclofenac is excreted unchanged, leading to bioaccumulation. When combined with other pharmaceuticals, this can significantly enhance its toxic effects, potentially accumulating in the tissues of organisms [18,23–27].

Given the current challenges in eliminating emerging contaminants and the increasing demand for potable water quality, many wastewater treatment plants (WWTPs) are compelled to upgrade their facilities by integrating new technologies [28,29].

Advanced Oxidation Processes (AOPs) are a prominent technological solution, generating highly reactive species such as hydroxyl radicals (HO^\bullet), which can effectively eliminate resistant or toxic molecules [30–32].

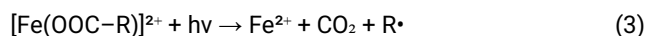
Among these processes, Fenton and photo-Fenton reactions are notable for their high efficiency in terms of decontamination and disinfection. The treatment is based on the production of hydroxyl radicals (HO^\bullet), as shown in reactions 1 and 2.



One major disadvantage is the need to adjust the pH to 2.8 (highly acidic) to prevent iron precipitation. Additionally,

irradiation between 320 – 400 nm with an ideal wavelength of 354 nm, is required for regeneration [29]. These ideal conditions limit the effectiveness of Fenton and photo-Fenton reactions, making improvements necessary [33,34]. On the other hand, these processes offer broad degradation action for emerging contaminants, low cost, simple application, and minimal environmental impact [29,31,33,35,36].

The addition of carboxylic acids (OOCR), such as citric acid and oxalic acid, is advantageous due to their excellent ability to form photoactive complexes with Fe^{3+} . These compounds can undergo photolysis, leading to the reduction of Fe^{3+} to Fe^{2+} (reaction 3) [5,37–39].



This reaction enhances the regeneration of soluble iron, thereby improving efficiency of Fenton reactions [18,31,33]. Moreover, the formation of these complexes can prevent precipitation, providing a significant advantage to the Fenton-based process. These complexes are also soluble at near-neutral pH, avoiding the need for adjustments to acidic conditions (pH 2.5 – 3.0), which is one of the main limitations of the classical Fenton method. Furthermore, the presence of these complexing agents can contribute to more efficient reactions, reducing the formation of undesirable sub products that may result from the decomposition of hydrogen peroxide [40,41].

The use of organic complexing agents in Fenton and photo-Fenton reactions represents a promising strategy for pollutant degradation, particularly when combined with solar irradiation. Complexing agents, such as citrate, improve UV-Vis light sensitivity, enhancing catalytic reaction efficiency. This approach not only reduces the need for artificial energy sources, promoting resource savings, but also aligns with sustainability principles by utilizing renewable inputs and minimizing environmental impacts, making the process viable for large-scale applications [36,42–44].

Monitoring the toxicity of sub products formed after photocatalytic treatment is crucial for evaluating the safety and effectiveness of the process, ensuring environmental safety. It also helps optimize operational conditions for treatment systems and develop mitigation strategies to minimize adverse impacts. Therefore, it is essential to ensure the efficiency and sustainability of photocatalytic water and wastewater treatment processes [31,45–47].

This study aimed to assess the efficiency of Fenton and photo-Fenton reactions enhanced by organic complexing agents in mitigating emerging contaminants, with a focus on sodium diclofenac (SDF).

2. Results and Discussion

2.1 Effect of addition of organic complexing agents

The influence of citrate and oxalate addition is presented in the comparative results of SDF photodegradation, using Fenton and photo-Fenton reactions (Figure 1).

The oxidative photodegradation reaction operates under steady-state, maintaining a high concentration of hydroxyl radicals (HO^\bullet) within the reaction medium. These radicals interact with the diclofenac molecule, competing for available electrons and disrupting its molecular bonds, ultimately leading to degradation [30, 31, 44, 48]. The reaction rate equation is presented in Equation 1.

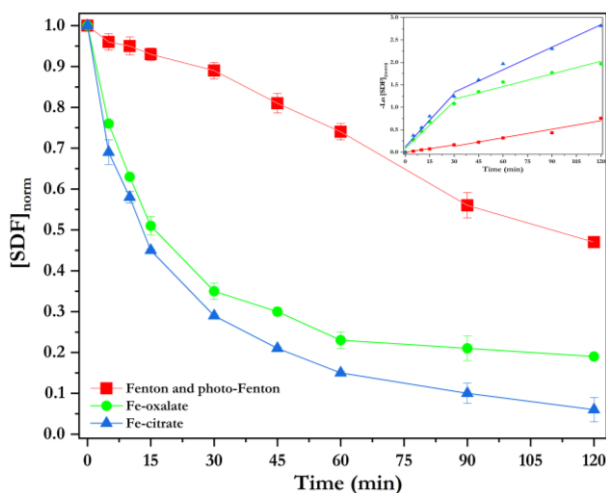


Fig. 1. Photodegradation of SDF. Inset: Estimation of rate constant.

$$r = k[\text{SDF}][\cdot\text{OH}] \quad \text{Eq. 1}$$

Seeing that $[\cdot\text{OH}] \gg [\text{SDF}]$, the kinetics reaction can be adjusted (Equation 2).

$$r = k_{\text{app}} [\text{SDF}] \quad \text{Eq. 2}$$

where, $k_{\text{app}} = k[\cdot\text{OH}]$, getting a pseudo-first order kinetic [30,31,44,48]. The rate law of the pseudo-first order kinetic is integrated in order to obtain a relation between the concentration of diclofenac present in the photocatalytic process in function of time (Equation 3):

$$-\ln \frac{[\text{SDF}]}{[\text{SDF}]_0} = k_{\text{app}} t \quad \text{Eq. 3}$$

From these results presented, the photodegradation performance values and rate constant estimation were estimated (Figure 2).

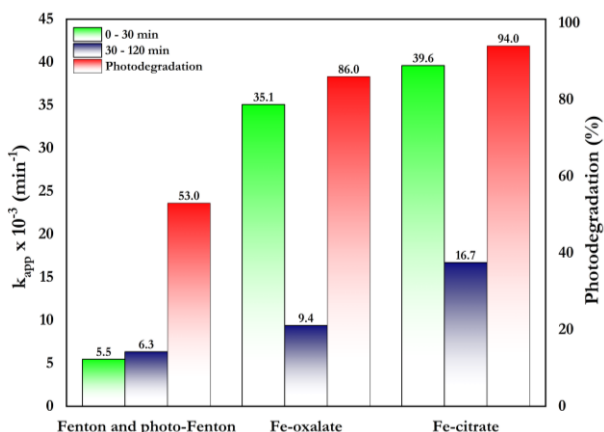


Fig. 2. Photocatalytic performance of Fenton and photo-Fenton tests

The results indicate the favorable influence of organic complexing agents, significantly boosting the photocatalytic performance of Fenton and photo-Fenton reactions. Especially with the Fe-citrate complex, as it indicates a higher SDS photodegradation rate, reaching 94.0 %.

In the study of kinetic estimation (k_{app}), in the range of 0 – 30 min, the test with citrate addition was superior by 623.95 % compared to the Fenton and photo-Fenton test and superior by 9.30 % compared to the test with oxalate addition. For the range of 30 – 120 min, the test with citrate addition was superior by 136.98 % compared to the Fenton and photo-Fenton test and superior by 77.95 % compared to the test with oxalate addition.

The influence of organic complexing agents on the observed photocatalytic performance in Fenton and photo-Fenton reactions is clarified in figure 3.

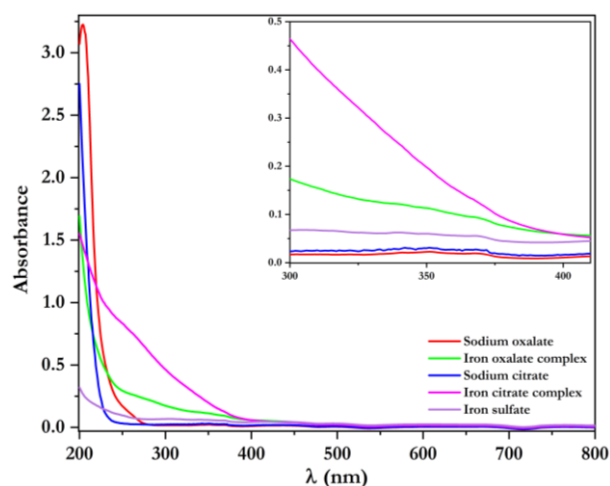


Fig. 3. UV - vis absorption spectrum. Inset: Absorption in the 300 - 400 nm region.

The results from the scans performed indicate that the presence of ferric citrate (Fe-citrate) and ferrioxalate (Fe-oxalate) complexes significantly enhances absorption in the UV and visible regions, as evidenced by comparing the absorption values with those of the individual reagents. Figure 3 (inset) further demonstrates that these complexes, particularly ferrioxalate and ferric citrate, increase absorption in the visible light region, especially near 400 nm. This behavior clearly enhances the efficiency of Fenton and photo-Fenton reactions within these spectral regions [49].

In addition to demonstrating superior performance in UV-vis light absorption, the Fe-citrate complex is a promising alternative for enhancing iron solubility in Fenton and photo-Fenton processes. Although its photolysis yields a lower quantum efficiency for Fe^{2+} generation compared to ferrioxalate, citrate is less toxic, readily available, and can be used at higher pH levels than oxalate (up to pH 9.0) [32]. Notably, the use of organic ligands eliminates the need for acidification and neutralization steps, reducing costs and facilitating large-scale applications. While an increase in carbon load may be a potential drawback, the complete conversion of organic ligands to CO_2 ensures no net increase in carbon emissions [41].

2.2 Experimental factorial design

Factorial design has been used in several studies involving AOPs in order to study the influence of each variable in the process, and from there find the best conditions to achieve higher performances for pollutant removal [47,50–54]. The results obtained with the proposed design are presented in Table 1.

Table 1. Experimental factorial design for the photodegradation of SDF.

Factors	(-)	(+)		
1: pH	4.0	7.0		
2: Citrate:Fe ²⁺	0.1	1.0		
3: Light source	LED	Hg		
Test	1	2	3	Photodegradation (%)
1	-	-	-	39.6 ± 0.1
2	+	-	-	37.3 ± 0.4
3	-	+	-	49.3 ± 2.1
4	+	+	-	45.9 ± 1.0
5	-	-	+	60.2 ± 0.8
6	+	-	+	57.3 ± 0.3
7	-	+	+	95.8 ± 0.7
8	+	+	+	91.5 ± 0.6

Initially, it is pertinent to analyze the influence of the radiation sources. In this context, tests 1–4 (LED) and 5–8

(Hg) present results under the proposed conditions that indicate improved outcomes with Hg vapor lamps. Furthermore, based on the photoactivity profile shown in Figure 3 (Absorption spectrum of the complexes), it is evident that the Fe-Citrate complex enhances absorption capacity in the visible region, with significant activity in the UV region. The Hg vapor lamp emits within the 200–600 nm spectral range, with prominent peaks at ≈ 380 , 550, and 600 nm,[55] while the LED lamp emits exclusively white light, operating in the 400–800 nm range, with peaks at ≈ 450 , 500, and 750 nm [56]. This broader spectral coverage and photon availability underline the superior performance of the Hg vapor lamp, as it emits in regions that align closely with the Fe-Citrate complex's highest photoactivity, thereby enhancing Fenton and photo-Fenton reactions. [57] Using a radiometer, irradiance measurements of the lamps used in the tests were obtained, as shown in Table 2.

Table 2. UV and visible irradiance dose.

Time (min)	UV	LED (kJm ⁻²) Visible	Total	UV	Hg (kJm ⁻²) Visible	Total
0	0	0	0	0	0	0
30	0.01	31.46	31.47	17.47	24.08	41.56
60	0.03	61.50	61.53	37.25	50.77	88.02
90	0.04	91.22	91.26	55.68	76.33	132.02
120	0.05	121.35	121.40	75.42	103.21	178.63

The results present irradiance measurements as a function of SDF photodegradation time. The LED lamp used emits virtually no UV radiation, although its emission in the visible light region is considerably strong. As previously noted, the Hg vapor lamp records emissions covering both the UV and visible regions from the beginning of the experiment.

The total irradiance dose values for both lamps over 120 minutes were relatively close, contrasting with the notably different photocatalytic performance results. The Fe-citrate complex enhances absorption in the visible region and significantly boosts absorption in the UV range, which may favor Fenton and photo-Fenton reactions. Although LED lamp experiments (tests 1–4) achieved less than 50% SDF photodegradation within the parameters analyzed, the photocatalytic performance is promising when considering the lamp's low power, low energy consumption, and visible-region-exclusive emission. Thus, when using artificial light sources, cost is a crucial factor, particularly for batch-scale treatment projects. [28,31,51,52,58] Several studies support the application LED, emphasizing that ongoing advancements in materials may enable broader adoption of this type of emission source. [26,33,53,59]

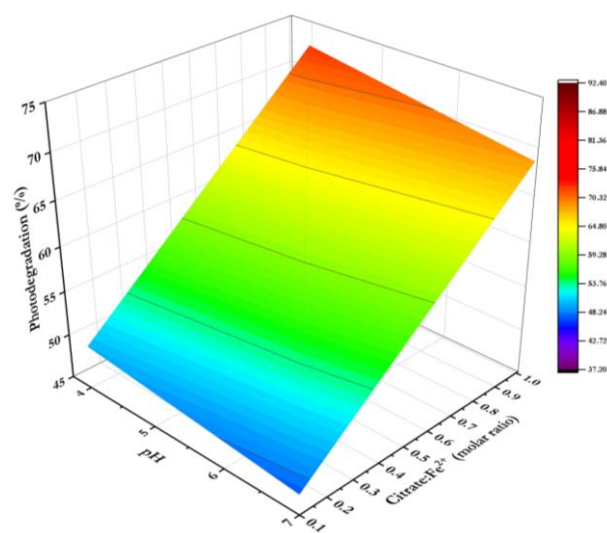
Based on the factorial design results (table 1), considering factors, pH and the Citrate:Fe²⁺ molar ratio, the influence on photocatalytic performance is illustrated in Figure 4.

The analysis of the response surface suggests that increasing the amount of citrate in the molar proportion reinforces the trend of a significant improvement in the efficiency of Fenton and photo-Fenton SDF photodegradation, attributed to the presence of the Fe-citrate complex. This effect can be explained by the photoactivity of the complex, which generates Fe²⁺ with a relatively high quantum yield [37].

Regarding the influence of pH in the medium, it is observed that the response surface indicates better photocatalytic performance at a pH close to 4, with a decrease in efficiency at a pH near 7. As pH increases, the Fe(OH)Cit⁻ species becomes predominant, exhibiting lower photoactivity, with the

quantum yield for Fe²⁺ generation ranging from 0.28 to 0.21 within the pH range of 4–6 at 436 nm [57].

This factor may explain the reduction in SDF degradation at higher pH levels. However, even with an increase in pH, the quantum yields of Fe-citrate complexes remain higher than those observed for the Fe(OH)²⁺ complex, the main Fe³⁺ species in solution in the presence of FeSO₄ and absence of citrate, which has a quantum yield of 0.017 ± 0.003 at 360 nm [60–62]. When comparing the performance of tests 7 (pH 4.0) and 8 (pH 7.0) (Table 1), a difference of only 4.5% is observed. Thus, it is advantageous to operate at a pH near neutral, minimizing the need for pH adjustments in the process [31].

**Fig. 4.** Response surface for photodegradation of SDF.

2.3. Solar photodegradation

Solar energy is a highly abundant, sustainable, and clean resource. In the western region of Bahia, Brazil (latitude: -12.1482, longitude: -44.9925), annual solar irradiation ranges

from 5000 to 6250 kWhm⁻²day⁻¹, indicating excellent availability. Additionally, the solar spectrum consists of about 3–5% UV and approximately 47% visible light. [30,36,42,44,51]

The high availability of solar radiation enhances the performance of photo-Fenton reactions, especially when Fe-citrate complexes are present. Table 3 presents the solar irradiance measurements obtained.

Table 3. Solar UV (A and B) and visible (global) irradiance dose.

Time (min)	UV (kJm ⁻²)	Visible (kJm ⁻²)
0	0	0
39	100.0	172.42
74	200.0	347.54
103	300.0	4934.0
132	400.0	6522.7
160	500.0	8059.8
189	600.0	9586.0
217	700.0	11125.0
248	800.0	12678.0
276	900.0	14231.0
311	1000.0	15993.5

The measured values indicate a predominance of radiation in the visible region and high energy availability over approximately 5 hours of measurements (311 min). When comparing irradiance doses, the energy measured for visible radiation is approximately 16 times greater than that measured for UV radiation, equivalent to a 1600% increase. This high availability of UV and visible radiation is a regional characteristic, suggesting the feasibility of sunlight as an energy source for this type of reaction.

The advantages are numerous, including: the use of a sustainable and abundant energy source, which reduces dependence on artificial light sources and, consequently, lowers costs; greater availability of visible light, which enhances the activation of photo-Fenton reactions facilitated by the presence of Fe-citrate complexes; and, in areas with high radiation incidence, potentially even higher efficiency, leading to faster degradation of contaminants. Furthermore, large-scale applicability is possible due to the constant availability of solar radiation, enabling the feasibility of batch treatment systems, such as CPC reactors, for effluent treatment or wastewater decontamination [2,18,23,36,44,57,63–66]. Figure 5 presents the results of the solar photodegradation tests.

Based on these results, photodegradation performance values and rate constant were estimated (Figure 6).

The results indicate that the addition of citrate enhances the Fenton and photo-Fenton reactions, leading to a 29.14% increase in photodegradation performance. In the kinetic study, for the ranges of 0–500 kJm⁻² and 500–1000 kJm⁻², the tests with citrate addition showed superior performances of 73.13 % and 94.73 %, respectively, compared to the Fenton and photo-Fenton tests without citrate.

The data further support the photodegradation efficiency of SDF at 89.25 %, demonstrating that the presence of the Fe-citrate complex improves the photocatalytic processes, particularly under intense sunlight exposure, with a focus on radiation in the visible region. This approach enables more efficient utilization of solar radiation. Although the process requires more time to achieve this level of performance, the results underscore the significance of utilizing solar radiation in photocatalytic reactions.

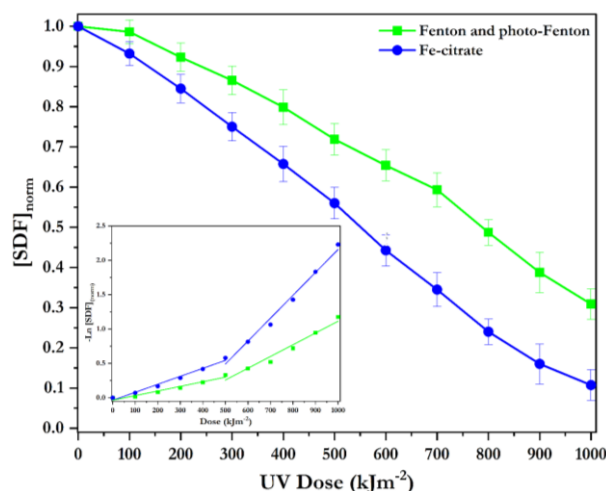


Fig. 5. Solar photodegradation of SDF. Inset: Rate constant (k_{app}).

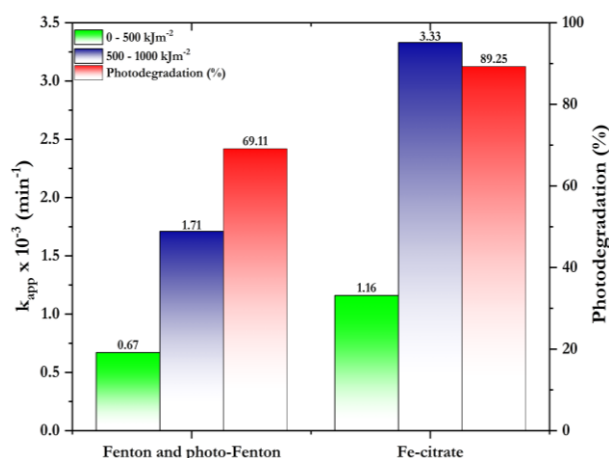


Fig. 6. The photocatalytic performance of Fenton and photo-Fenton tests, with and without the presence of citrate.

2.4 Mineralization and removal of SDF

The efficiency of the drug mineralization process, i.e., the conversion of organic carbon present in the SDF molecule, was evaluated by the decay of the total organic carbon concentration. TOC information relates the sum of all organically bound carbons in dissolved and undissolved organic species [67]. The results of TOC concentrations are presented in Figure 7.

The results indicate that the mineralization of SDF was more efficient when subjected to Fenton and photo-Fenton processes with the addition of citrate, achieving a performance of 82.0 %, whereas the photocatalytic assays without citrate achieved only 62.0 %. Thus, the addition of citrate contributed to a 32.3 % increase in performance. The mineralization of the drug is of great importance as it reflects the trend of eliminating this emerging contaminant, which has a stable molecular structure and a high capacity for accumulation in the environment. Furthermore, it indicates the drug's susceptibility to exposure to both conventional and innovative treatments. The major challenge today is the elimination of not only the contaminants but also their by-products [27, 68, 69].

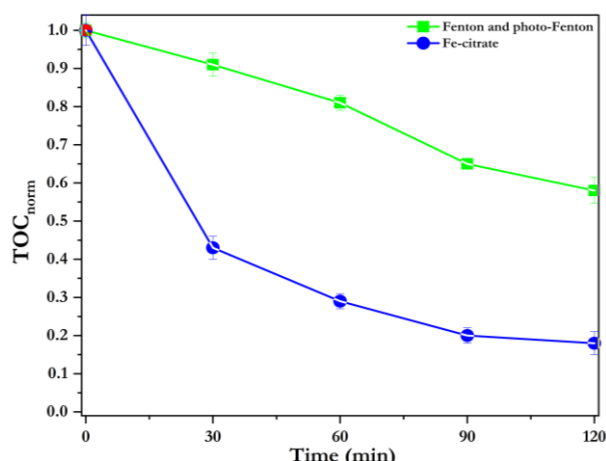


Fig. 7. TOC reduction by SDF photodegradation.

2.5 Evolution of acute toxicity

The toxicity analysis using *Artemia salina* is essential for evaluating the environmental impact of waste generated from photocatalytic tests. This bioassay allows verification of whether the byproducts resulting from pollutant degradation retain any residual toxicity, thereby ensuring the ecological safety of the process. Additionally, the simplicity and low cost of the test make it accessible for continuous monitoring. This assay also provides a rapid initial assessment of acute toxicity, offering relevant data for improving effluent treatment technologies.

Previous results obtained under the same experimental conditions indicate that the lethal concentration (LC) is estimated at $4.41 \times 10^{-4} \text{ mol L}^{-1}$ [70]. Thus, the concentration of SDF used in the photodegradation tests is slightly above this value. The results of the toxicity assessment of the SDF samples collected after the photodegradation tests are presented in Table 4.

Table 4. Counting of surviving *artemias Salinas*.

Photodegradation time (min)	Fenton and photo-Fenton (survivor count)	Fe-citrate (survivor count)
Blank	10 ± 0.0	10.0 ± 0.0
0	2.67 ± 0.57	2.67 ± 0.57
30	4.33 ± 0.57	6.66 ± 0.57
60	7.32 ± 0.57	8.33 ± 0.57
90	8.33 ± 0.57	8.66 ± 0.57
120	8.66 ± 0.57	10.0 ± 0.0

From the values presented and using equation 4, the toxicity values (%) were estimated (Figure 8).

$$\text{Toxicity (\%)} = 100 - \left(\frac{\text{Surviving} \times 100}{\text{Blank}} \right) \quad \text{Eq. 4}$$

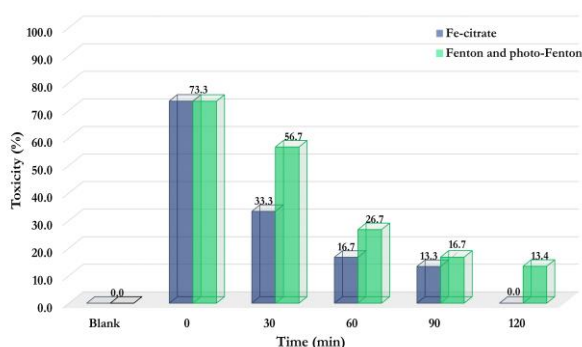


Fig. 8. Estimated toxicity reduction of SDF samples as a function of photodegradation time.

The results indicate that the photodegradation tests utilizing the Fenton and photo-Fenton processes were effective in reducing the toxicity of SDF residues, particularly with the addition of citrate. Within a period of 30 minutes, the toxicity was reduced by 40.0 %, achieving a total reduction over 120 minutes, which demonstrates the effectiveness of the treatment. This notable reduction indicates that the sub products generated after treatment are not lethally toxic to the organisms tested.

3. Material and Methods

3.1 Materials

Deionized (DI) water was supplied by Milli-Q Water system, iron sulphate heptahydrate ($\text{FeSO}_4 \cdot 7\text{H}_2\text{O}$, 99.0%, Sigma-Aldrich), sodium oxalate ($\text{Na}_2\text{C}_2\text{O}_4$, 99.0%, Vetec); sodium citrate ($\text{Na}_3\text{C}_6\text{H}_5\text{O}_7$, 99.0%, Isosfar); hydrogen peroxide (H_2O_2 , 50% w/v, Sigma-Aldrich); methanol (CH_3OH , HPLC analytical-grade; Sigma-Aldrich); sodium diclofenac (SDF) (99.9%, local pharmacy); sea salt and *Artemia salina* eggs, commercially obtained.

3.2 Basic experimental setup

The bench-scale Fenton and photo-Fenton tests followed a basic experimental setup: $[\text{SDF}] = 4.5 \times 10^{-4} \text{ mol L}^{-1}$ (100 mg L^{-1}), temperature between 40 and 45 °C, $[\text{H}_2\text{O}_2] = 0.5 \text{ mol L}^{-1}$, a high-pressure Hg lamp (125 W), and an irradiation time of 120 minutes. For the Fenton and photo-Fenton tests, $[\text{Fe}^{2+}] = 2.7 \times 10^{-4} \text{ mol L}^{-1}$ (15.0 mg L^{-1}) [71], pH = 3.0 – 3.5, and a borosilicate glass photocatalytic reactor with a volume of 2 L were used. An illustration of the photocatalytic system setup is shown in Figure 9.

3.3 Effect of the addition of organic complexing agents

The influence of organic complexing agents, oxalate and citrate, on Fenton and photo-Fenton reactions was evaluated using the following concentrations: $[\text{C}_2\text{O}_4^{2-}] = 2.72 \times 10^{-4} \text{ mol L}^{-1}$, $[\text{C}_6\text{H}_5\text{O}_7^{3-}] = 2.72 \times 10^{-4} \text{ mol L}^{-1}$. The other parameters for the photocatalytic tests followed the basic experimental setup.

3.4 Experimental factorial design

An experimental design was proposed to evaluate the influence of the following parameters: pH, citrate: Fe^{2+} molar ratio, and irradiation sources including LED (50 W) and high-pressure Hg vapor lamp (125 W). Table 5 shows the 2^3 factorial design adopted.

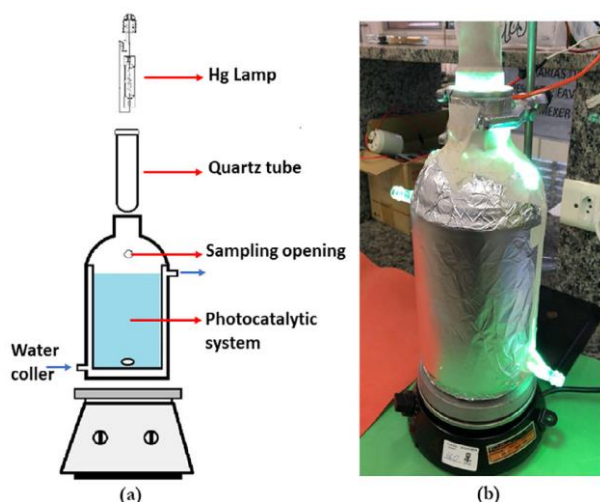


Fig. 9. a. Schematic of the photocatalytic system; b. Photocatalytic reactor [72].

Table 5. Factorial design 2³.

Parameters	(-)	(+)	
1: pH	4.0	7.0	
2: Citrate:Fe ²⁺	0.1	1.0	
3: Light source	LED	Hg	
Tests	1	2	3
1	-	-	-
2	+	-	-
3	-	+	-
4	+	+	-
5	-	-	+
6	+	-	+
7	-	+	+
8	+	+	+

The citrate:Fe²⁺ molar ratio was proposed by varying the amount of citrate and keeping the amount of Fe²⁺ constant.

3.5 Solar photodegradation tests

The tests were conducted from June to September, characterized by the absence of rain and low cloud cover. Fenton and photo-Fenton reactions were tested with and without citrate addition. The basic experimental setup was used for the Fenton and photo-Fenton tests without citrate. For the tests with citrate addition, a citrate:Fe²⁺ molar ratio of 1:1 and pH of 7.0 were used. The SDF solution was added to a 2.0 L borosilicate beaker and kept under constant stirring with a magnetic stirrer (Figure 10).



Fig. 10. Schematic of the photocatalytic system for solar tests.

Sample collections were conducted at every 100 kJm⁻² of accumulated UV radiation dose (A and B) until reaching a total dose of 1000 kJ m⁻², with the aid of a radiometer (SOLAR-LIGHT, model PMA2100). Additionally, visible radiation doses (global) were measured in parallel. Other parameters followed the basic experimental setup.

3.6 Chemical analyses

The concentration of SDF samples collected during photodegradation assays was monitored using HPLC-UV under the following experimental conditions: wavelength of 282 nm, column temperature of 30 °C, a C18 reversed-phase column (3.5 µm, 150 mm × 4.6 mm), and a water/methanol mobile phase in a ratio of 80:20, using isocratic elution with a flow rate of 0.50 mL min⁻¹, a running time of 15 min, and an injection volume of 50 µL.

Total organic carbon (TOC) analysis is used to estimate the efficiency of the photodegradation process in promoting the mineralization of SDF samples. The equipment (TOC- L analyser, Shimadzu) is based on CO₂ quantification through non-dispersive infrared analysis after high-temperature catalytic combustion. The tests were performed with and without the presence of citrate. The experimental setup consisted of a citrate:Fe²⁺ molar ratio of 1:1 and a pH of 7.0. Other parameters followed the basic experimental setup.

3.7 Toxicity assay

The acute toxicity of treated and non-treated SDF samples was determined by monitoring the mortality of *Artemia salina*. This well-established procedure is widely used in research,[46,70,73,74] due to its several advantages, such as low cost, excellent sensitivity to toxic substances, and rapid response. It is extensively utilized to directly estimate real toxicity levels.

Following the methodology described in the literature,[70] *Artemia salina* cysts were incubated in an aquarium containing 20 gL⁻¹ of saline solution, illuminated with a 20 W lamp for 48 hours at room temperature (≈ 25 °C) (Figure 11).

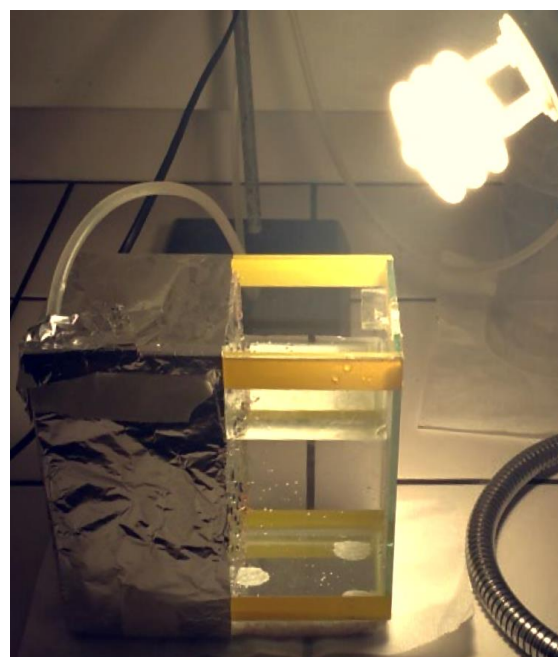


Fig. 11. *Artemia salina* cysts incubation system.

After the incubation period, ten nauplii were placed in 10 mL of each SDF sample collected during the photodegradation assays at 0, 30, 60, 90, and 120 minutes. This procedure was also performed with a reference sample (blank) consisting solely of saline solution. The samples containing the nauplii were maintained for 48 hours under light exposure and ambient temperature. At the end of the exposure period, the surviving organisms were counted to evaluate the toxicity of the SDF solutions.

4. Conclusions

This study demonstrated the effectiveness of organic complexing agents, particularly citrate, in enhancing Fenton and photo-Fenton reactions for the degradation of SDF. The Fe-citrate complex showed superior utilization of UV and visible light, and the experimental design confirmed the feasibility of using LED lamps as a sustainable and efficient irradiation source. Optimization revealed that citrate not only improved reaction performance but also enabled operation at near-neutral pH, maintaining high efficiency. Solar photodegradation tests further validated the approach, achieving significant degradation rates. Mineralization and toxicity reduction analyses supported these findings, indicating that the proposed methods are promising for mitigating environmental toxicity.

Acknowledgments

The authors gratefully acknowledge the financial support provided by the Coordination for the Improvement of Higher Education Personnel (CAPES) and the National Council for Scientific and Technological Development (CNPQ). We also thank the Federal University of Western Bahia (UFGB) for providing the infrastructure and academic environment necessary for this study. Special thanks are extended to Professor José D. S. Silva, Ph.D. (Cangaço Research Group) and Professor Paulo H. G. D. Diniz, Ph.D. (Research Group on Chemical and Chemometric Methods of Analysis) for their invaluable contributions. This work would not have been possible without the support of these institutions.

Author Contributions

Marcele Oliveira Silva developed the experimental activities to fulfill the requirements for obtaining a master's degree in Chemistry. Maiara Bernardes Marques contributed to writing, reviewing, submitting and discussing toxicity tests.

References and Notes

- [1] de Araújo, J. C.; Madeira, C. L.; Bressani, T.; Leal, C.; Leroy, D.; Machado, E. C.; Fernandes, L. A.; Espinosa, M. F.; Freitas, G. T. O.; Leão, T.; Mota, V. T.; Pereira, A. D.; Perdigão, C.; Tröger, F.; Ayrimoraes, S.; de Melo, M. C.; Laguardia, F.; Reis, M. T. P.; Mota, C.; Chernicharo, C. A. L. *Sci. Total Environ.* **2023**, 860, 160498. [\[Crossref\]](#)
- [2] Hernández-Tenorio, R.; González-Juárez, E.; Guzmán-Mar, J. L.; Hinojosa-Reyes, L.; Hernández-Ramírez, A. J. *Hazard. Mater. Adv.* **2022**, 8, 100172. [\[Crossref\]](#)
- [3] Gomes, M. P. *Phyton-International J. Exp. Bot.* **2024**, 93, 2127. [\[Crossref\]](#)
- [4] Kesic, R.; Elliott, J. E.; Lee, S. L.; Elliott, K. H. *Environ. Pollut.* **2024**, 363, 125099. [\[Crossref\]](#)
- [5] La Manna, P.; De Carluccio, M.; Iannece, P.; Vigliotta, G.; Proto, A.; Rizzo, L. *J. Hazard. Mater.* **2023**, 452, 131235. [\[Crossref\]](#)
- [6] Couto, C. F.; Lange, L. C.; Amaral, M. C. S. *J. Water Process Eng.* **2019**, 32, 100927. [\[Crossref\]](#)
- [7] Buerge, I. J.; Poiger, T.; Müller, M. D.; Buser, H. R. *Environ. Sci. Technol.* **2003**, 37, 691. [\[Crossref\]](#)
- [8] Kermia, A. E. B.; Fouial-Djebbar, D.; Trari, M. *Comptes Rendus Chim.* **2016**, 19, 963. [\[Crossref\]](#)
- [9] Nascimento, M. M.; Nascimento, M. L.; Pereira dos Anjos, J.; Cunha, R. L.; da Rocha, G. O.; Ferreira dos Santos, I.; Pereira, P. A. de P.; de Andrade, J. B. *J. Chromatogr. A* **2023**, 464230. [\[Crossref\]](#)
- [10] Huizer, M.; ter Laak, T. L.; de Voogt, P.; van Wezel, A. P. *Water Res.* **2021**, 207, 117789. [\[Crossref\]](#)
- [11] Alessandretti, I.; Rigueto, C. V. T.; Nazari, M. T.; Rosseto, M.; Dettmer, A. *J. Environ. Chem. Eng.* **2021**, 9, 106743. [\[Crossref\]](#)
- [12] Tabelini, D. B.; Lima, J. P. P.; Borges, A. C.; Aguiar, A. J. *Water Process Eng.* **2023**, 53, 103779. [\[Crossref\]](#)
- [13] Dires, S.; Birhanu, T.; Ambelu, A.; Sahilu, G. *J. Environ. Chem. Eng.* **2018**, 6, 4265. [\[Crossref\]](#)
- [14] Ren, L.; Liang, Z.; Yang, K.; Wang, Z.; Wang, Z.; Wang, Z.; Ma, J. *Adv. Technol. Wastewater Treat.* **2023**, 89. [\[Crossref\]](#)
- [15] Krzeminski, P.; Tomei, M. C.; Karaolia, P.; Langenhoff, A.; Almeida, C. M. R.; Felis, E.; Gritten, F.; Andersen, H. R.; Fernandes, T.; Manaia, C. M.; Rizzo, L.; Fatta-Kassinos, D. *Sci. Total Environ.* **2019**, 648, 1052. [\[Crossref\]](#)
- [16] Nogueira, A. A.; Souza, B. M.; Dezotti, M. W. C.; Boaventura, R. A. R.; Vilar, V. J. P. *J. Photochem. Photobiol. A Chem.* **2017**, 345, 109. [\[Crossref\]](#)
- [17] Nayak, A.; Chaudhary, P.; Bhushan, B.; Ghai, K.; Singh, S.; Sillanpää, M. *Int. J. Biol. Macromol.* **2024**, 258, 129092. [\[Crossref\]](#)
- [18] Zhang, T.; Liu, B.; Li, Q.; Niu, X.; Xia, Z.; Qi, L.; Liu, G.; Liu, Y.; Gao, A.; Wang, H. *Sep. Purif. Technol.* **2025**, 353, 128386. [\[Crossref\]](#)
- [19] Zhao, Y.; Wang, C.; Cao, X.; Song, S.; Wei, P.; Zhu, G. *Sci. Total Environ.* **2024**, 951, 175380. [\[Crossref\]](#)
- [20] Bodus, B.; O'Malley, K.; Dieter, G.; Gunawardana, C.; McDonald, W. *Sci. Total Environ.* **2024**, 906, 167195. [\[Crossref\]](#)
- [21] Sultan, M. B.; Anik, A. H.; Rahman, M. M. *Mar. Pollut. Bull.* **2024**, 199, 115982. [\[Crossref\]](#)
- [22] Available from: <https://www.statista.com/topics/5107/pharmaceutical-industry-in-brazil/#topicOverview>. January 2025.
- [23] Cardoso, R.; da Silva, T. F.; Cavalheri, P. S.; Machado, B. S.; Nazario, C. E. D.; Machulek Junior, A.; Sirés, I.; Gozzi, F.; de Oliveira, S. C. *J. Environ. Chem. Eng.* **2024**, 12, 112704. [\[Crossref\]](#)
- [24] Ebal, J. C. C.; Marchadesch, A. N. R.; Oro, R. A. G.; Ortega, R. M. P.; Polinar, P. J. B.; Bolaños, I. F. Y.; Halabaso, E.; Rubi, R. V. C.; Roque, E. C.; Lopez, E. C. R. *Mater. Today Proc.* **2023**. [\[Crossref\]](#)

- [25] Latif, S.; Liaqat, A.; Imran, M.; Javaid, A.; Hussain, N.; Jesionowski, T.; Bilal, M. *Environ. Res.* **2023**, 216, 114500. [\[Crossref\]](#)
- [26] Pizzichetti, R.; Reynolds, K.; Pablos, C.; Casado, C.; Moore, E.; Stanley, S.; Marugán, J. *Chem. Eng. J.* **2023**, 471, 144520. [\[Crossref\]](#)
- [27] Louadj, A.; Bouras, O.; Houari, S.; Ezzeroug, K.; Houari, M.; Kourdali, S. *Desalin. Water Treat.* **2024**, 317, 100119. [\[Crossref\]](#)
- [28] Gualda-Alonso, E.; Soriano-Molina, P.; Casas López, J. L.; García Sánchez, J. L.; Plaza-Bolaños, P.; Agüera, A.; Sánchez Pérez, J. A. *Appl. Catal. B Environ.* **2022**, 319, 121908. [\[Crossref\]](#)
- [29] Maniakova, G.; Rizzo, L. *J. Environ. Chem. Eng.* **2023**, 11, 111356. [\[Crossref\]](#)
- [30] Yuste-Córdoba, F. J.; Pérez-Salguero, C.; Santiago-Codosero, T.; Godoy-Cancho, B. *Results Eng.* **2024**, 102252. [\[Crossref\]](#)
- [31] Decker, J.; Le, T. T. M.; Entenza, J. M.; del Castillo Gonzalez, I.; Hernandez Lehmann, A.; Pulgarin, C.; Rodriguez-Chueca, J.; Giannakis, S. *J. Environ. Chem. Eng.* **2024**, 12, 112147. [\[Crossref\]](#)
- [32] Wang, R.; Chu, Y.; Zhang, H. *J. Environ. Chem. Eng.* **2024**, 12, 112479. [\[Crossref\]](#)
- [33] Delgado-Vargas, C. A.; Barreneche-Vasquez, J. S.; Cógua, N. G.; Botero-Coy, A. M.; Hernández, F.; Martínez-Pachón, D.; Moncayo-Lasso, A. *J. Environ. Chem. Eng.* **2023**, 11, 111030. [\[Crossref\]](#)
- [34] Linares-Hernández, I.; Antonio Castillo-Suárez, L.; Ibanez, J. G.; Vasquez-Medrano, R.; Miguel López-Rebollar, B.; Santoyo-Tepole, F.; Alejandra Teutli-Sequeira, E.; Martínez-Cienfuegos, I. G. *J. Photochem. Photobiol. A Chem.* **2022**, 429, 113914. [\[Crossref\]](#)
- [35] Djouider, F.; Banoqitah, E.; Alhawsawi, A. *Desalin. Water Treat.* **2024**, 317, 100118. [\[Crossref\]](#)
- [36] Wang, J.; Wang, X.; Zhang, Q.; Guo, L.; Zhang, Q.; Liu, Y.; Zeng, Q. *Sep. Purif. Technol.* **2025**, 354, 129233. [\[Crossref\]](#)
- [37] Delgado-Vargas, C. A.; Espinosa-Barrera, P. A.; Villegas-Guzman, P.; Martínez-Pachón, D.; Moncayo-Lasso, A. *Environ. Sci. Pollut. Res.* **2022**, 29, 42275. [\[Crossref\]](#)
- [38] Gomes, M. P.; Rocha, D. C.; Moreira de Brito, J. C.; Tavares, D. S.; Marques, R. Z.; Soffiatti, P.; Sant'Anna-Santos, B. F. *Ecotoxicol. Environ. Saf.* **2020**, 196, 110549. [\[Crossref\]](#)
- [39] Wang, Y.; Zheng, H.; Wang, Q.; Li, Y. *ACS ES T Water* **2024**. [\[Crossref\]](#)
- [40] Xiao, C.; Li, S.; Yi, F.; Zhang, B.; Chen, D.; Zhang, Y.; Chen, H.; Huang, Y. **2020**. [\[Crossref\]](#)
- [41] Machado, F.; Teixeira, A. C. S. C.; Ruotolo, L. A. M. *Int. J. Environ. Sci. Technol.* **2023**, 20, 13995. [\[Crossref\]](#)
- [42] Menon, K.; Lopis, A. D.; Choudhari, K. S.; Kulkarni, B.; Maradur, S.; Kulkarni, S. D. *Mater. Res. Bull.* **2025**, 181, 113074. [\[Crossref\]](#)
- [43] Wang, R.; Chu, Y.; Zhang, H. *J. Environ. Chem. Eng.* **2024**, 12, 112479. [\[Crossref\]](#)
- [44] Clemente, E.; Domingues, E.; Quinta-Ferreira, R. M.; Leitão, A.; Martins, R. C. *Sci. Total Environ.* **2024**, 912, 169471. [\[Crossref\]](#)
- [45] Russo, C.; Nugnes, R.; Orlo, E.; di Matteo, A.; De Felice, B.; Montanino, C.; Lavorgna, M.; Isidori, M. *Environ. Pollut.* **2023**, 335, 122251. [\[Crossref\]](#)
- [46] Amutha, V.; Aiswarya, D.; Deepak, P.; Selvaraj, R.; Tamilselvan, C.; Perumal, P.; Balasubramani, G. *South African J. Bot.* **2023**, 152, 230. [\[Crossref\]](#)
- [47] Cavalheri, P. S.; Machado, B. S.; da Silva, T. F.; Warszawski de Oliveira, K. R.; Magalhães Filho, F. J. C.; Nazário, C. E.; Cavalcante, R. P.; de Oliveira, S. C.; Junior, A. M. *J. Environ. Chem. Eng.* **2023**, 11, 110699. [\[Crossref\]](#)
- [48] Gualda-Alonso, E.; Pichel, N.; Soriano-Molina, P.; Olivares-Ligero, E.; Cadena-Aponte, F. X.; Agüera, A.; Sánchez Pérez, J. A.; Casas López, J. L. **2023**. [\[Crossref\]](#)
- [49] Dou, J.; Alpert, P. A.; Arroyo, P. C.; Luo, B.; Schneider, F.; Xto, J.; Huthwelker, T.; Borca, C. N.; Henzler, K. D.; Raabe, J.; Watts, B.; Herrmann, H. *Atmos. Chem. Phys.* **2021**, 21, 315. [\[Crossref\]](#)
- [50] Giménez, B. N.; Conte, L. O.; Alfano, O. M.; Schenone, A. V. *J. Photochem. Photobiol. A Chem.* **2020**, 397, 112584. [\[Crossref\]](#)
- [51] Hinojosa, M.; Oller, I.; Quiroga, J. M.; Malato, S.; Egea-Corbacho, A.; Acevedo-Merino, A. *Environ. Sci. Pollut. Res.* **2023**, 30, 96208. [\[Crossref\]](#)
- [52] Martín de Vidales, M. J.; Prieto, R.; Galán-Lucarelli, G.; Atanes-Sánchez, E.; Fernández-Martínez, F. *Catal. Today* **2023**, 413, 1. [\[Crossref\]](#)
- [53] González-Rodríguez, J.; Conde, J. J.; Vargas-Osorio, Z.; Vázquez-Vázquez, C.; Piñeiro, Y.; Rivas, J.; Feijoo, G.; Moreira, M. T. *J. Environ. Manage.* **2024**, 349, 119461. [\[Crossref\]](#)
- [54] Kanmaz, N.; Buğdaycı, M. *J. Mol. Struct.* **2024**, 1295, 136718. [\[Crossref\]](#)
- [55] Gindl, M.; Sinn, G.; Stanzl-Tschegg, S. E. *J. Adhes. Sci. Technol.* **2006**, 20, 817. [\[Crossref\]](#)
- [56] Oliveira, C. H. L. de; Costa, M. A. D.; Costa, G. H. *XXIV Congr. Bras. Eng. Biomédica – CBEB* 2014, 1.
- [57] Farinelli, G.; Giannakis, S.; Schaub, A.; Kohantorabi, M.; Pulgarin, C. *Water Res.* **2024**, 255, 121518. [\[Crossref\]](#)
- [58] Marson, E. O.; Ricardo, I. A.; Paniagua, C. E. S.; Ueira-vieira, C.; Starling, M. C. V. M.; Antonio, S.; Trov, A. G. *Molecules* **2022**, 27, 5521. [\[Crossref\]](#)
- [59] Wang, W.; Xie, H.; Li, G.; Li, J.; Wong, P. K.; An, T. *ACS ES T Water* **2021**, 1, 1483. [\[Crossref\]](#)
- [60] Martín-Sómer, M.; Vega, B.; Pablos, C.; van Grieken, R.; Marugán, J. *Appl. Catal. B Environ.* **2018**, 221, 258. [\[Crossref\]](#)
- [61] Belikov, Y. A.; Snytnikova, O. A.; Grivin, V. P.; Plyusnin, V. F.; Xu, J.; Wu, F.; Pozdnyakov, I. P. *Chemosphere* **2022**, 309, 136657. [\[Crossref\]](#)
- [62] Conte, L. O.; Schenone, A. V.; Alfano, O. M. *Environ. Sci. Pollut. Res.* **2017**, 24, 6205. [\[Crossref\]](#)
- [63] Alkorbi, A. S.; Muhammad Asif Javed, H.; Hussain, S.; Latif, S.; Mahr, M. S.; Mustafa, M. S.; Alsaiani, R.; Alhemiary, N. A. *Opt. Mater. (Amst.)* **2022**, 127, 112259. [\[Crossref\]](#)
- [64] Mugundan, S.; Praveen, P.; Sridhar, S.; Prabu, S.; Lawrence Mary, K.; Ubaidullah, M.; Shaikh, S. F.;

- Kanagesan, S. *Inorg. Chem. Commun.* **2022**, 139, 109340. [\[Crossref\]](#)
- [65] Nandana, B.; John, S.; Velmaiel, K. E.; Nambi, I. M.; Thomas, T.; Singh, S. *J. Environ. Chem. Eng.* **2024**, 12, 111567. [\[Crossref\]](#)
- [66] Hafedh, A.; Mohammed, M.; Park, J.; Öztürk, A. *International Journal of Mechanical and Production Engineering* **2018**, 6, 2320. [\[Link\]](#)
- [67] Hiram, Y.; Hunge, Y. M.; Suzuki, N.; Rodríguez-González, V.; Kondo, T.; Yuasa, M.; Fujishima, A.; Teshima, K.; Terashima, C. *J. Colloid Interface Sci.* **2023**, 642, 829. [\[Crossref\]](#)
- [68] Martín de Vidales, M. J.; Prieto, R.; Galán-Lucarelli, G.; Atanes-Sánchez, E.; Fernández-Martínez, F. *Catal. Today* **2023**. [\[Crossref\]](#)
- [69] Rahman, M. M.; Sultan, M. B.; Alam, M. *Curr. Opin. Environ. Sci. Heal.* **2023**, 31, 100420. [\[Crossref\]](#)
- [70] Souza, D. R.; Galdino, M.; Lima, L. da S. *Orbital* **2022**, 14, 221. [\[Crossref\]](#)
- [71] De Souza, D. R.; De Miranda, J. A.; Ribeiro, K. R.; Mapeli, A. M.; Santos, D. D. J. *Orbital - Electron. J. Chem.* **2016**, 1. [\[Crossref\]](#)
- [72] Souza, D. R.; Neves, J. V. S.; França, Y. K. S.; Malheiro, W. C. *Photochem. Photobiol.* **2021**, 97, 32. [\[Crossref\]](#)
- [73] Carolina de Almeida, M.; Machado, M. R.; Costa, G. G.; de Oliveira, G. A. R.; Nunes, H. F.; Maciel Costa Veloso, D. F.; Ishizawa, T. A.; Pereira, J.; Ferreira de Oliveira, T. *Heliyon* **2023**, 9, 11. [\[Crossref\]](#)
- [74] Swarnkumar Reddy; Osborne, W. J. *Biocatal. Agric. Biotechnol.* **2020**, 25, 101574. [\[Crossref\]](#)

How to cite this article

Silva, M. O.; Marques, M. B.; Souza, D. R. *Orbital: Electronic J. Chem.* **2025**, 17, 70. DOI: <http://dx.doi.org/10.17807/orbital.v17i1.22735>